

Short Communication

Experimental Research of Anticorrosion Performance of Steel with Ni-Sn-P Coating

Jie Yang¹, Xiaodong Zhao^{1,2,*}, Jie Zhang^{3,*}, Weijie Fan¹, Qingchao Li¹, Chaoming Yan¹

¹School of Naval Architecture and Ocean Engineering, Zhejiang Ocean University, Zhoushan 316022, China;

²Key Laboratory of Offshore Engineering Technology of Zhejiang Province, Zhoushan 316022, China;

³Key Laboratory of Marine Environmental Corrosion and Bio-fouling, Institute of Oceanology, Chinese Academy of Sciences, Qingdao 266071, China

*E-mail: danielxdzhao@aliyun.com; zhangjie@qdio.ac.cn

Received: 23 March 2015 / Accepted: 14 April 2015 / Published: 28 April 2015

In this work, an improved plating solution was prepared aiming at improving the utilization rate of effective components and reducing the content of hypophosphite in the plating solution to some extent. Considering the variation of complex reductant in the plating solution, the performance of the coating was evaluated by various electrochemical measurements, including potentiodynamic polarization curves and electrochemical impedance spectroscopy, and surface characterization. It was found that the coating resulted from proper addition of complex reductant was able to effectively serve as a barrier layer to block corrosive species from reaching the steel surface.

Keywords: Chemical plating; Complex reductant; Potentiodynamic polarization; AC impedance; Deposition rate

1. INTRODUCTION

Nickel-based chemical plating is widely used for surface treatment since last century because of its excellent wear resistance, corrosion resistance, weldability and optical performance. Compared with electroplating, bright and dense alloy coating can be easily performed on various surface such as glasses, plastics, ceramics, and metals without external electric field[1~3].

To further improve the thermal stability and other important properties, the third element such as Sn, Cu or Sb is usually introduced in the Ni-P based binary alloy to form a ternary alloy for the change of crystallization behavior of the Ni-P ternary alloys. Documents give examples that Ni-Sn-P coating shows more excellent performance in many applications than Ni-Sn coating[4~8]. Jeon et al[9]

studied the deposition mechanism of formation of Ni-Sn-P alloy coating produced by Ni-P alloys reacting with Sn-Pb and Sn-Ag respectively in solder using transmission electron microscopy (TEM). Research of Wang et al[10] showed that Sn-Ni-P alloy rods array electrode had high reversible capacity and excellent coulombic efficiency with its tiny pinhole defect structure. Zhang et al[11] confirmed the ternary Ni-Sn-P coating exhibited better corrosion resistance than the Ni-P coating in protecting the magnesium alloy substrate by electrochemical performance tests and SEM analysis. However, at present, the reductant commonly used for Ni-Sn-P ternary plating solution comprises mainly hypophosphite, resulting in a large number of substances which are difficult to dispose, for example phosphoric acid, in the waste liquid. How to deal with the waste liquid is still a problem for the development of chemical plating.

In the present study, an improved complex reductant composed of glucose, glycine and sodium hypophosphite was prepared and adopted in the plating solution, aiming at improving the utilization rate of effective components in the plating solution and reducing the hypophosphite to some extent. Influence of the content of complex reductant on electrochemical performance and microstructure of Ni-Sn-P alloy coating was investigated to optimize the components associated with corresponding performance.

2. EXPERIMENTAL SECTION

2.1 Coating Preparation

Table 1. Process of Ni-Sn-P coating preparation

Step	operation		ingredients	condition
1	Pre-treatment	sanding		SiC abrasive paper, step by step to 1000#
2		alkaline cleaning	NaOH 50g/l, Na ₃ PO ₄ ·12H ₂ O 15g/l	40°C, 2min
3		acid cleaning	Dilute sulfuric acid 150ml/l, nitric acid 10ml/l	Room temperature, 2min
4		Activation	dilute sulfuric acid 50ml/l	30°C, 10min
5		Water cleaning	Distilled water	
6	Plating		NiSO ₄ 22 g/l, SnCl ₄ 3.5 g/l, complex reductant 23 g/l, Sulfoarea ≤0.0008 g, Na ₂ S ₂ O ₃ 2.5 g/l, C ₂ H ₄ O ₂ 7g/l	Temperature:85~93°C pH: 4.5~5.5 Time:3h
7	Modification		Myristic acid in ethanol solution, 22.83 g/l	Time:5~6d

*Complex reductant is composed of glucose(45%), glycine(0.1%) and sodium acetate(54.9%).

The size of Q235 steel specimens to be plated was 20mm×40mm×2mm, processed according to the requirements in table 1. Specimens were cleaned by water between each two operations within 2 min, then placed in a desiccator and ready for use after all the operations.

Each component was weighed accurately according to the formula, and the plating solution was prepared after the complete dissolution of the mixture in 1000mL distilled water. The solution was heated to 85°C by magnetic stirrer, acetic acid and sodium bicarbonate were used to adjust the pH value to 4.5~5.5, then the plating was performed according to the 4.0dm²/l loading ratio. After plating, samples were cooled down to room temperature and then thickness at five different locations of the coating were measured using MINITEST-600 thickness gauge and averaged to calculate the deposition rate.

2.2 Electrochemical Measurements

The electrochemical measurements were conducted with a PARSTAT 2273 electrochemical workstation in a conventional three-electrode cell system, where the coating sample and a platinum wire were used as working electrode and counter electrode, respectively. A saturated calomel electrode (SCE) coupled with a Luggin capillary was used as reference electrode. The testing solution was clean seawater derived from East China Sea area. Each test was usually conducted three times to confirm reproducibility of the data. Potentiodynamic polarization curves were recorded from -0.35 to +0.25 V/SCE versus corrosion potential at a scan rate of 20 mV/min. The EIS measurements were carried out at open-circuit potential (OCP) with the frequency range from 100 kHz to 0.01 Hz and an AC disturbance potential of 0.01 V.

2.3 Morphological Characterization

Surface of the coating samples were washed and dried, and then Zeiss Ultra 55 type scanning electronic microscope (SEM) was used for microscopic morphological characterization.

3. RESULTS AND DISCUSSION

3.1 Deposition Rate Measurement

As shown in Fig.1, deposition rate gradually increased at first, reached a maximum of 37μm/h and then decreased with the increment of complex reductant content.

According to the atomic hydrogen theory proposed by Brenner and Riddell[12], during the plating deposition process, atomic hydrogen as a catalyst is usually provided by hydrolysis of hypophosphite (Formula 1). The reduction of nickel and tin ions (Formula 2, 3) and deposition of phosphorus (Formula 4) can be realized by atomic hydrogen.

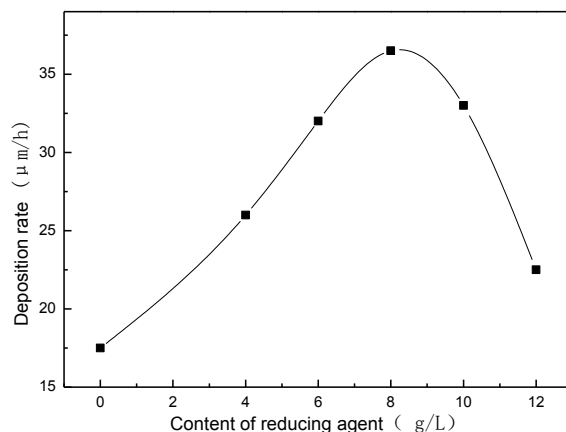


Figure 1. Correlation between reductant content and deposition rate

However, in real reaction a portion of hydrogen is generated (Formula 5) and phosphorus deposition is usually formed (Formula 6). As the reductant, the efficiency of hypophosphite is reduced to about 35% due to the two processes.



The mechanism of the complex reductant used in present study is to improve reduction efficiency by producing more atomic hydrogen by hydrolysis and inhibiting the alkaline hydrolysis process of hypophosphite[13~15]. In the same condition of other components and plating, with increase of complex reductant, the number of free atomic hydrogen increased in the solution, and Ni^{2+} and Sn^{2+} ions would be reduced by sufficient hydrogen atoms to the deposition of Ni and Sn on the catalytic coating surface. As the main source of phosphorus deposition (Formula 7), hypophosphite greatly increased the deposition rate in some content range. With excess complex reductant, the hydrolytic process of hypophosphite was excessively inhibited, and precipitation of nickel phosphite with smaller solubility product was generated, leading to the decrease of the deposition rate.

3.2 Polarization Curve Measurements

Potentiodynamic polarization curves with variation of reductant content were shown in Fig.2 and fitting parameters were analyzed and shown in Tab.2 and Fig.3.

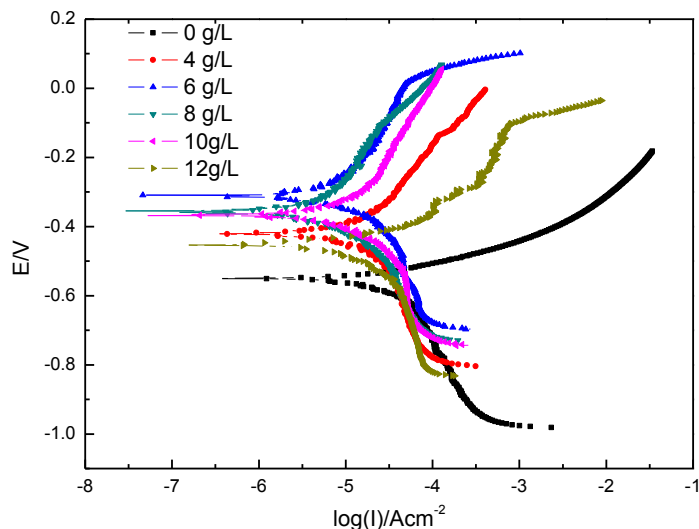


Figure 2. Correlation between reductant content and potentiodynamic polarization curves

Table 2. Electrochemical corrosion parameters derived from polarization curves measured in Fig. 2, where E_{corr} is corrosion potential, and b_a and b_c are anodic and cathodic Tafel slopes

content of reductant (g/l)	b_a (mV/dec)	b_c (mV/dec)	I_{corr} (A/cm^2)	E_{corr} (V/SCE)	Corrosion Rate (mm/a)
0	310.38	389.2	$2.4567E-5$	-0.5480	0.28901
4	297.27	609.62	$1.9106E-5$	-0.38295	0.22472
6	360.73	185.22	$8.5136E-6$	-0.31313	0.10014
8	283.38	211.73	$5.1564E-6$	-0.33643	0.06065
10	407.37	286.01	$1.2433E-5$	-0.36423	0.14623
12	139.45	714.4	$2.5381E-5$	-0.42929	0.29854

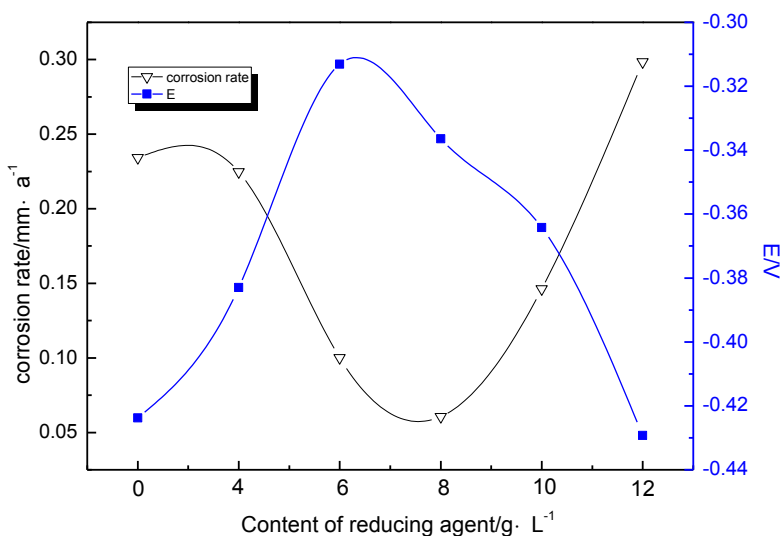


Figure 3. Relationship between corrosion rate, E_{corr} and the reductant content

It was shown in Fig.3 that firstly with the increasing content of complex reductant, the corrosion potential of coating shifted in positive direction gradually while the corrosion rate decreased. The corrosion potential rose to -0.31313V and corrosion rate reached a minimum of 0.06065mm/a in the 6~8g/l content range. The coating generated served as a physical barrier for corrosive medium and the anodic polarization was inhibited during the process. When the content continued to increase, the corrosion potential began to shift in the opposite direction and the corrosion rate increased. With excess complex reductant, content of Ni^{2+} , Sn^{2+} free ions decreased by complex formation and the main salt Ni^{2+} ions in the reductant solution were hindered from reaching the catalytic surface, affecting the precipitation process of Ni. Deposition thickness and the coverage of alloy were reduced and anodic dissolution was enhanced at the same polarization, resulting in the negative shift of corrosion potential and increase of the corrosion current(corrosion rate).

3.3 EIS Measurements

In order to characterize the mechanistic aspect of the effect of coating on corrosion process, EIS measurements were conducted on steel specimens with different reductant contents in plating solution, as shown in Fig. 4. According to the theory of AC impedance and with the help of software Z-view, equivalent circuit in Fig. 5 was used for curve fitting and parameters were shown in table 3. The CPE was used in the circuit instead of capacitance due to the in-homogeneous coating.

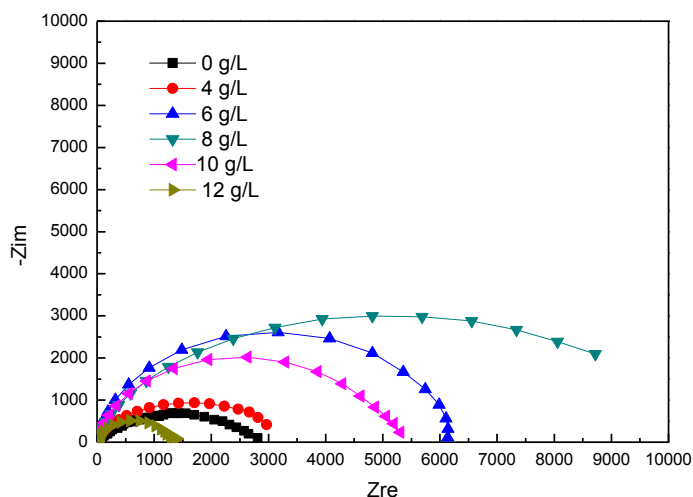


Figure 4. Nyquist diagram by AC impedance measurement of coating

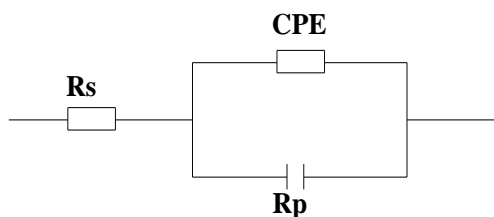


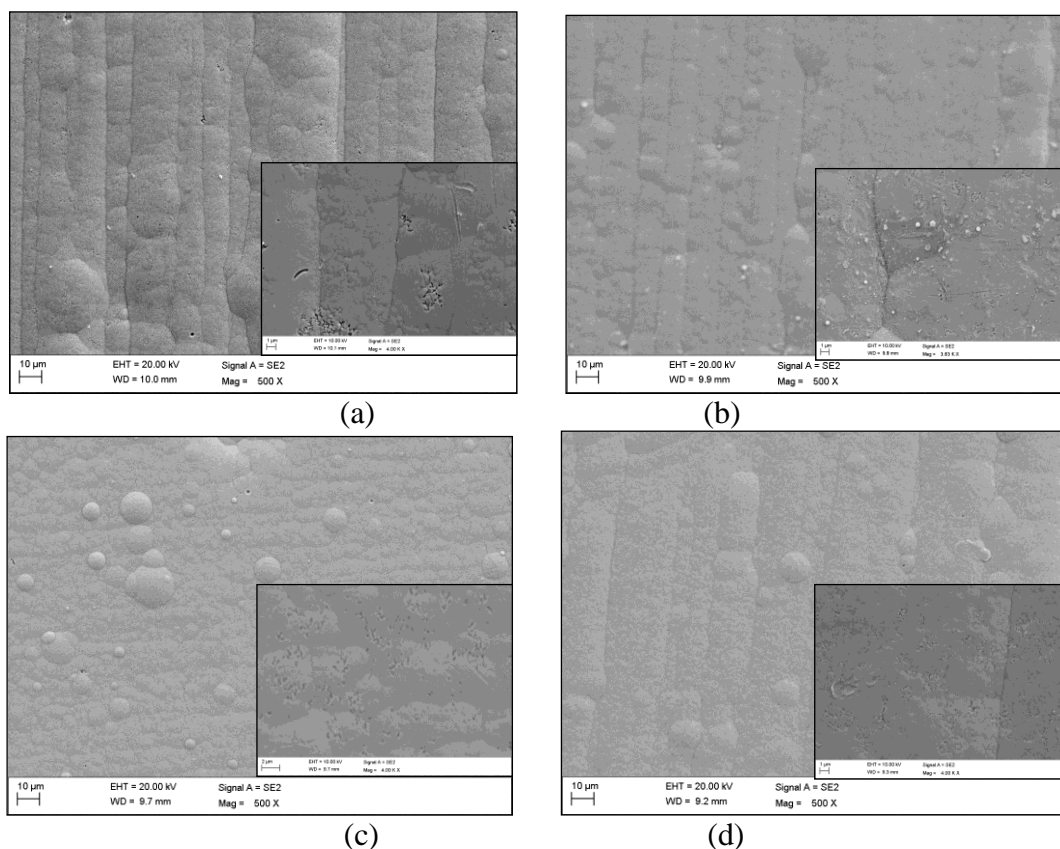
Figure 5. Equivalent circuit diagram used for curve fitting

Table 3. Fitting parameters derived from AC impedance diagram in Fig.4

Content of reducing agent (g/l)	R_s ($\Omega \cdot \text{cm}^{-2}$)	R_p ($\Omega \cdot \text{cm}^{-2}$)	CEP-T ($\mu\text{F} \cdot \text{cm}^{-2}$)	CEP-p ($\mu\text{F} \cdot \text{cm}^{-2}$)
0	17.03	9454	6.3213E-5	0.81071
4	17.42	10590	6.9427E-5	0.82646
6	18.45	24270	2.6571E-5	0.92669
8	14.89	31000	3.5699E-5	0.86291
10	16.78	19942	3.1645E-5	0.90006
12	12.19	5195	3.9272E-5	0.88551

Incomplete and depressed semicircles were observed in the whole frequency range in Fig.4. Moreover, the size of the semicircle reached a maximum with a reductant content of 8g/l and decreased whether with a lower or a higher content. Generally, the size of the semicircle is related to charge-transfer resistance of corrosion reaction occurring at the electrode/solution interface, and determined by the thickness of the surface coating[16]. The biggest semicircle associated with a maximum of R_p , $31\text{K}\Omega \cdot \text{cm}^{-2}$, according to table 3, revealed a thickest coating and an outstanding corrosion resistance. Thickness and integrity of coating resulted from lower or higher content of reductant in coating solution were influenced and the sizes of the semicircle were comparatively smaller. The result of EIS measurements also indicated the optimized content of reductant.

3.4 Morphological Characterization



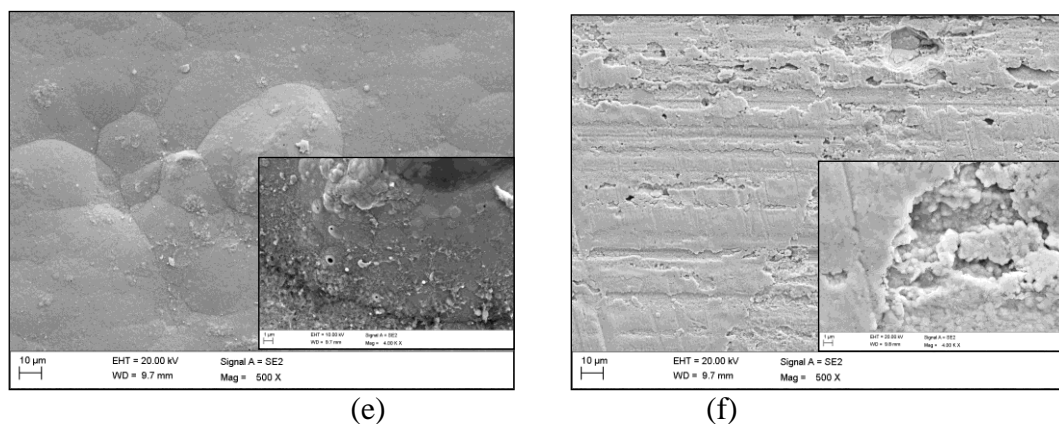


Figure 6. Coating morphological characterization induced by different reductant content (a) 0g/l, (b) 4g/l, (c) 6g/l, (d) 8/l, (e) 10g/l, (f) 12g/l

Fig.6 (c) and (d) show the coatings are uniform and compact, and the surface is smooth. Corrosion resistance of amorphous alloy was generally better than that of crystalline alloy and the performance also varies due to the crystal structure. The proper addition of complex reductant changed the microstructure of coating, promoted the formation of amorphous alloy and reduced the defects on the surface[17~19]. However, with insufficient or excessive complex reductant, shown in Fig. 6 (a), (b), (e) and (f), the surface is rough, loose and full of pinhole defects or microparticles, indicating that the coating may not be sufficient to resist the corrosion.

4. CONCLUSION

A chemical plating solution is prepared with optimized content of complex reductant, enabling a compact and smooth coating surface generated on the steel surface, which can protect the steel from corrosion attack in seawater. The formed coating is primarily composed of amorphous alloy, serving as an effective barrier layer to block aggressive species in the solution from reaching the steel substrate. Moreover, the deposition rate of the coating is also elevated with optimized composition.

ACKNOWLEDGMENTS

This research was supported by State Key Laboratory of Ocean Engineering (Shanghai Jiao Tong University) (Grant No.1406). The support from Program of Bureau of Science and Technology Department of Zhoushan(2013C41003) and Zhejiang Provincial Natural Science Foundation of China under Grant No. Q14D060002 is also gratefully acknowledged.

Reference

1. Y. D. He, H. F. Fu, X. G. Li, *Scripta. Mater.*, 58(2008)504.
2. Y. C. Lin, T. Y. Shih, S. K. Tien, *Scripta. Mater.*, 56(2007)49.

3. L. Luo, Y. Wu, J. Li, *Surf. Coat. Tech.*, 206(2011)1091.
4. Z. P. Xia, Y. Lin, Z. Q. Li, *Mater. Charact.*, 59(2008)1324.
5. A. Kumar, M. He, Z. Chen, *Thin. Solid. Films.*, 462(2004)413.
6. J. Yu, T. Jing, J. Yang, *J. Mater. Process. Tech.*, 209(2009)14.
7. P. Sun, C. Andersson, X. Wei, *J. Alloy. Compd.*, 437(2007)169.
8. J. F. Li, S. H. Mannan, M. P. Clode, *Acta. Mater.*, 55(2007)737.
9. Y. D. Jeon, K. W. Paik, K. S. Bok, *Electronic Components and Technology Conference*, (2001)1326.
10. Y. X. Wang, L. Huang, Y. Q. Chang, *Electrochem. Commun.*, 12(2010)1226.
11. W. X. Zhang, Z. H. Jiang, G. Y. Li, *Surf. Coat. Tech.*, 202(2008)2570.
12. A. Brenner, G. E. Riddell, *J. Res. Natl. Bureau. Stand.*, 37(1946)31.
13. W. Riedel, *Electroless Ni Plating*, ASM International, Finishing Publications (1991) p.1.
14. D. Mencer, *J. Alloys Compd.*, 306 (2000) 158
15. J. S. Lian, G. Y. Li, L. Y. Niu, *Surf. Coat. Technol.*, 200 (2006) 5956.
16. S. Faraji, A. A. Rahim, N. Mohamed, *Arab. J. Chem.*, 6(2013)379.
17. D. O. Ovono, I. Guillot, D. Massinon, *J. Alloys Compd.*, 432 (2006) 241.
18. W. Y. Chen, S. K. Tien, F. B. Wu, J. G. Duh, *Surf. Coat. Technol.*, 182 (2004) 85.
19. F. Liu, H. F. Wang, Z. Chen, *J. Mater. Lett.*, 60 (2006) 3916.

© 2015 The Authors. Published by ESG (www.electrochemsci.org). This article is an open access article distributed under the terms and conditions of the Creative Commons Attribution license (<http://creativecommons.org/licenses/by/4.0/>).